HHS Public Access

Author manuscript

AAPS J. Author manuscript; available in PMC 2020 May 01.

Published in final edited form as:

AAPS J. ; 22(2): 51. doi:10.1208/s12248-020-0421-z.

Physiologically Based Pharmacokinetic Modeling and Tissue Distribution Characteristics of SHetA2 in Tumor-Bearing Mice

Ankur Sharma[1], **Mengjie Li**[1], **Elangovan Thavathiru**[2], **Mariam Ibrahim**[1], **Lucila Garcia-Contreras**[1], **Doris M Benbrook**[2,3], **Sukyung Woo**[1,3,4]

[1]Department of Pharmaceutical Sciences, College of Pharmacy, The University of Oklahoma Health Sciences Center, Oklahoma City, Oklahoma, USA

[2]Department of Obstetrics and Gynecology, College of Medicine, The University of Oklahoma Health Sciences Center, Oklahoma City, Oklahoma, USA

[3]Peggy and Charles Stephenson Cancer Center, The University of Oklahoma Health Sciences Center, Oklahoma City, Oklahoma, USA

Abstract

The orally available novel small molecule SHetA2 is the lead sulfur-containing heteroarotinoid that selectively inhibits cancer cells over normal cells, and is currently under clinical development for anticancer treatment and cancer prevention. The objective of this study was to assess and characterize the tissue distribution of SHetA2 in tumor-bearing mice by developing a physiologically based pharmacokinetic (PBPK) model. An orthotopic SKOV3 ovarian cancer xenograft mouse model was used to most accurately mimic the ovarian cancer tumor microenvironment in the peritoneal cavity. SHetA2 concentrations in plasma and 14 different tissues were measured at various time points after a single intravenous dose of 10 mg/kg and oral dose of 60 mg/kg, and these data were used to develop a whole-body PBPK model. SHetA2 exhibited a multi-exponential plasma concentration decline with an elimination half-life of 4.5 h. Rapid and extensive tissue distribution, which was best described by a perfusion rate–limited model, was observed with the tissue-to-plasma partition coefficients (k_p = 1.4–21.2). The PBPK modeling estimated the systemic clearance (76.4 mL/h) from circulation as a main elimination pathway of SHetA2. It also indicated that the amount absorbed into intestine was the major determining factor for the oral bioavailability (22.3%), while the first-pass loss from liver and intestine contributed minimally (< 1%). Our results provide an insight into SHetA2 tissue distribution characteristics. The developed PBPK model can be used to predict the drug exposure

[4]To whom correspondence should be addressed. (skwoo@buffalo.edu).

AUTHORS' CONTRIBUTIONS

Participated in research design: Sharma, Woo, and Benbrook

Conducted experiments: Sharma, Thavathiru, Ibrahim, Woo, and Benbrook

Contributed new reagents or analytical tools: Sharma, Woo, and Benbrook

Performed data analysis: Sharma, Li, and Woo

Wrote or contributed to the writing of the manuscript: Sharma, Li, Ibrahim, and Woo

Reviewed and edited the writing of the manuscript: Sharma, Li, Thavathiru, Ibrahim, Garcia-Contreras, Woo, and Benbrook

Electronic supplementary material The online version of this article (https://doi.org/10.1208/s12248-020-0421-z) contains supplementary material, which is available to authorized users.

at tumors or local sites of action for different dosing regimens and scaled up to humans to correlate with efficacy.

Keywords

PBPK model; SHetA2; tissue distribution

INTRODUCTION

SHetA2, [[(4-nitrophenyl) amino][2,2,4,4-tetramethyl thiochroman-6-yl)amino] methane-1-thione] (1) is a sulfur heteroarotinoid anticancer drug that belongs to the class of flexible heteroarotinoids (Flex-Hets). It functions independent of the retinoic acid receptors, and causes potent induction of apoptosis in cancer cells, without harming normal cells (2).

SHetA2 induced G1 cell arrest and apoptosis in human ovarian cancer cells with a half maximum concentration (IC_{50}) of ~ 0.37–4.6 μM for growth inhibition in the National Cancer Institute 60 cell line screen (3), and also inhibited the growth of ovarian and kidney xenograft tumors at oral doses of 10–60 mg/kg (1,3–7). Extensive preclinical studies of SHetA2 demonstrated a lack of mutagenicity or teratogenicity (8,9). SHetA2 had a wide therapeutic window with a no-observed-adverse-effect level (NOAEL) of > 1500 mg/kg/day in a 28-day dog toxicity study (10). These tumor-selective activities and broad safety profile make SHetA2 an ideal drug for cancer prevention and treatment strategies (11).

SHetA2 is highly hydrophobic and has low oral absorption with poor bioavailability (< 1%) in rats when administered in an aqueous solution (10) and 12–19% in mice and dogs when administered with a formulation aid (10,12). Given the favorable *in vivo* pharmacokinetic profiles allowing for once or twice-a-day dosing (13) and low toxicity (10), improved SHetA2 formulations can overcome the low bioavailability concern. A better understanding of the tissue distribution of SHetA2 in tumor-bearing mice is imperative in determining whether SHetA2 concentrations at the target sites can modulate the molecular target leading sufficiently to produce an optimal pharmacodynamic response. This information will help us predict drug exposure at target organs in humans in future clinical trials. Physiologically based pharmacokinetic (PBPK) modeling can greatly facilitate a basic understanding of dose- and time-exposure relationships and factors contributing to drug absorption, distribution, metabolism, and excretion (ADME) at various steps of drug movement in the body. PBPK modeling integrates physiological parameters, such as blood flow and tissue sizes, and drug-specific parameters to simulate drug disposition in plasma and tissues (14). Since SHetA2 has poor solubility and possesses complex absorption and metabolism/degradation processes (13), PBPK modeling will be best suited to understanding SHetA2 pharmacokinetics. The objectives of the present study were (i) to study the tissue distribution in tumor-bearing mice following a single oral and intravenous administration of SHetA2 formulation and (ii) to quantitatively characterize drug absorption and disposition of SHetA2 using a PBPK model.

MATERIALS AND METHODS

Chemicals and Reagents

SHetA2 was provided by the National Cancer Institute RAPID Program. Internal standard (2, 3-Diphenylquinoxaline) was purchased from Acros Organics (New Jersey) and HPLC grade acetonitrile (HPLC-JT9012) was procured from VWR (Radnor, PA). Kolliphor HS 15 was obtained from Sigma-Aldrich (St. Louis, MO). Sterile phosphate-buffered saline (PBS) was purchased from Global Cell Solutions (Charlottesville, VA).

Cells

SKOV3, a human ovarian cell line, stably expressing firefly luciferase (SKOV3-luc) was a generous gift from Dr. Anil Sood (MD Anderson Cancer Center, Houston, TX). The cells were cultured in RPMI 1640 medium (Mediatech, Manassas, VA) supplemented with 10% fetal bovine serum (Serum Source International; Charlotte, NC) and 1% antibiotic-antimycotic (Thermo Fisher Scientific, Waltham, MA). For injection into mice, the cells were harvested, washed once with Hank's balanced salt solution (HBSS; Ca^{2+}, Mg^{2+}, and phenol-red-free), and re-suspended in HBSS (Thermo Fisher Scientific).

Orthotopic Xenograft Mouse Model

Crl: NU(NCr)-Foxn1nu 6-to-8-week-old female athymic nude mice (15–20 g) were purchased from Charles River Laboratories (Houston, TX). Mice were housed in a temperature-controlled room on a normal 12-h light/dark cycle, with free access to water and standard laboratory food. All procedures were approved and performed according to a protocol in compliance with Institutional Animal Care and Use Committee (IACUC) of the University of Oklahoma Health Sciences Center. After acclimatization for 1 week, the animals were injected intraperitoneally (i.p.) with one million SKOV3-Luc cells per animal. Tumor development was monitored at weeks 1 and 3 by imaging the animals using a Carestream In-vivo Xtreme imaging system (Carestream Molecular Imaging, CT) after i.p. injection with 125 μl of D-luciferin (30 mg/ml) purchased from Caliper Life Sciences (Waltham, MA). The net bioluminescence intensity was measured to derive tumor burden. In this model, 85–90% of animals developed tumors by week three.

Tissue Distribution of SHetA2 in Tumor-Bearing Mice

Two pharmacokinetic studies were conducted. For intravenous (i.v.) administration, 2.5 mg/ml of SHetA2 was prepared in 10% Kolliphor EL: sterile PBS v/v and filtered using 0.2-μm polypropylene Captiva ND plates, (Part # A5969002, Agilent Technologies, Santa Clara, CA), 1-ml Captiva 96-deep well collection plates (Part # A696001000), and a CaptiVac vacuum collar (Part # A796). For oral (p.o.) administration, SHetA2 formulation was prepared in 30% Kolliphor HS 15. SHetA2 was first finely triturated using a mortar and pestle to reduce its particle size from 300 to 400 μm to approximately less than 200 μm (15). The triturated SHetA2 was added to Kolliphor melted at 60°C and homogenized. Preheated deionized water was added stepwise to the mixture until reaching 30% Kolliphor (w/w). The resulting suspension was then homogenized under high-shear (Omni International, Kennesaw GA) for 2 min or more until the particle size <30 μm, measured by laser

diffraction (HELOS, Sympatec GmbH, Germany). The final concentration of SHetA2 suspension was 6 mg/ml to provide an oral dose of 60 mg/kg when administered with a dosing volume of 10 ml/kg.

In the first experiment, forty-five tumor-bearing mice were randomized into 15 groups of three mice that each received a single dose of 60 mg/kg SHetA2 suspension by oral gavage. At each time point, three mice underwent deep isoflurane anesthesia to collect blood from the inferior vena cava and were then euthanized to collect tissue samples, including tumor, lung, abdominal adipose tissues, skin, muscle, heart, kidneys, brain, uterus, fallopian tubes and ovaries, liver, spleen, and intestine. The sampling points included pre-dosing, 0.25, 0.5, 1, 1.5, 2, 2.5, 3, 4, 6, 8, 12, 24, 36, and 48 h after oral dosing. We collected all visible tumor nodules from the peritoneal cavity and weighed them together.

In the second experiment, twenty-one tumor-bearing mice were randomized into seven groups of three mice each and received 10 mg/kg SHetA2 solution i.v. via eye vein (100 μl adjusted by body weight). Similar to the oral study, blood and tissues were collected from three mice at each time point: pre-dosing and 0.25, 0.5, 1, 2, 4, 18, and 24 h after dosing. At 5 min and 12 h after i.v. dosing, additional blood was collected via saphenous vein (200 μl) under appropriate restraint conditions from three mice of the 18 and 24 h group. Whole-blood samples were collected in heparinized tubes and centrifuged immediately at 1200g for 10 min at 4°C to separate plasma. Tissue samples were rinsed in phosphate-buffered saline and blotted on tissue papers to remove any residual blood, weighed, and immediately frozen in liquid nitrogen, and stored at −80°C until analysis.

Quantification of SHetA2 in Plasma and Mouse Tissues

SHetA2 concentrations in plasma specimens were determined using the HPLC-UV method developed and validated in our laboratory (16). The method was validated across a range of 5–1000 ng/ml for SHetA2 in plasma, with a lower limit of quantification of 5 ng/ml. Briefly, 90 μl of mouse plasma sample was mixed with 10 μl of 5 μg/mL of internal standard (2, 3-diphenylquinoxaline) and the mixture was precipitated with 80 μl of chilled acetonitrile. The mixture was vortexed vigorously for 10 min and centrifuged at 21,381g for 15 min at 4°C. The supernatant was collected and filtered by Captiva filtration by applying a vacuum of not more than 5 in. of Hg. The filtrate was then injected (70 μl) and analyzed using a HPLC/UV system (Agilent 1260).

For 14 tissue samples, calibration curves were generated for each tissue using corresponding untreated tissues based on their size (Table SI). For generation of calibration curves, untreated tissues were thawed under ice in glass tubes and homogenized (Polytron™ 1600 EW benchtop homogenizer, Kinematica) with 3 ml/g chilled phosphate buffer (pH 7.4) submerged in an ice water bath. The 225 μl of homogenate was then spiked with 25 μl of master stock solution of 100 μg/ml SHetA2 in acetonitrile to generate 10 μg/ml standard which was further diluted with homogenate to prepare 1000 ng/ml of working standard. Serial dilutions were done to prepare different standards (Table SI). Tissue samples were extracted similar to the method described above for mouse plasma and calibration curves were prepared (Figure S1).

PBPK Model Development

The PBPK model (Fig. 1) was based on whole-body structure comprising of perfusion-limited compartments parameterized by tissue volumes (V_{tissue}), blood flow rates (Q_{tissue}), and the drug-dependent tissue/blood partition coefficient (K_{tissue}). The model includes 14 tissue compartments (lungs, heart, kidneys, spleen, ovaries/fallopian tubes, uterus, tumor, adipose tissue, brain, liver, muscle, intestine, skin, and carcass) that are linked by the blood flow. The PBPK model comprises a series of mass balance differential equations describing the concentration of SHetA2 in various tissues. The physiological values for mouse organ weights were either weighed or collected from literature. Most blood flow values were obtained from Gastroplus (SimulationsPlus Inc., Lancaster, CA) or literature (Table I) (17–19), whereas blood flows of tumor (Q_{TUM}) and adipose tissue (Q_{AD}) were obtained as the best-fitting values. Also, tumor volume (V_{TUM}) was estimated from the model fitting. It was assumed that the animal physiology and drug transport kinetics in tumor-bearing mice were identical to those in non-tumor-bearing mice.

SHetA2 was shown to be metabolized in liver microsomes (CL_{LIV}) and decomposed (CL_{PL}) in the both arterial and venous blood (12,20), possibly by the cleavage of the thiourea connected to the fused ring moiety. Similarly to the liver metabolism, intrinsic intestinal clearance (CL_{GI}) was also added to account for likely gut metabolism during oral absorption.

The arterial concentration was the output from the lungs. The input into the venous pool was the sum of the outputs from all tissues except lung. It was assumed that the drug undergoes similar decomposition (CL_{PL}) in both venous and arterial blood, contributing to overall plasma clearance. The venous blood volume was fixed to be 67% of total blood volume.

Artery (ART):

$$\frac{d}{dt}\mathrm{ART} = Q_{\mathrm{LU}} \bullet \left(\frac{C_{\mathrm{LU}}}{K_{\mathrm{LU}}} - \frac{\mathrm{ART}}{V_{\mathrm{ART}}}\right) - CL_{\mathrm{PL}} \bullet \frac{\mathrm{ART}}{V_{\mathrm{ART}}} \quad ; \quad \mathrm{ART}(0) = 0 \tag{1}$$

Venous pool (VEN):

$$\begin{aligned}\frac{d}{dt}\mathrm{VEN} = {} & Q_{\mathrm{LIV}} \bullet \frac{C_{\mathrm{LIV}}}{K_{\mathrm{LIV}}} + Q_{\mathrm{FTOV}} \bullet \frac{C_{\mathrm{FTOV}}}{K_{\mathrm{FTOV}}} + Q_{\mathrm{UT}} \bullet \frac{C_{\mathrm{UT}}}{K_{\mathrm{UT}}} \\ & + Q_{\mathrm{BR}} \bullet \frac{C_{\mathrm{BR}}}{K_{\mathrm{BR}}} + \ + Q_{\mathrm{KID}} \bullet \frac{C_{\mathrm{KID}}}{K_{\mathrm{KID}}} + Q_{\mathrm{HR}} \bullet \frac{C_{\mathrm{HR}}}{K_{\mathrm{HR}}} + Q_{\mathrm{TUM}} \bullet \frac{C_{\mathrm{TUM}}}{K_{\mathrm{TUM}}} \\ & + Q_{\mathrm{MUS}} \bullet \frac{C_{\mathrm{MUS}}}{K_{\mathrm{MUS}}} + Q_{\mathrm{SK}} \bullet \frac{C_{\mathrm{SK}}}{K_{\mathrm{SK}}} + Q_{\mathrm{CAR}} \bullet \frac{C_{\mathrm{CAR}}}{K_{\mathrm{CAR}}} + Q_{\mathrm{AD}} \bullet \frac{C_{\mathrm{AD}}}{K_{\mathrm{AD}}} \\ & - Q_{\mathrm{LU}} \bullet \frac{\mathrm{VEN}}{V_{\mathrm{VEN}}} - CL_{\mathrm{PL}} \bullet \frac{\mathrm{VEN}}{V_{\mathrm{VEN}}}; \qquad \mathrm{VEN}(0) = 0\end{aligned} \tag{2}$$

Liver (LIV):

$$\frac{d}{dt}\mathrm{LIV} = (Q_{\mathrm{LIV}} - Q_{\mathrm{SP}} - Q_{\mathrm{G1}}) \bullet \frac{\mathrm{ART}}{V_{\mathrm{ART}}} + Q_{\mathrm{SP}} \bullet \frac{C_{\mathrm{SP}}}{K_{\mathrm{SP}}} + Q_{\mathrm{GI}} \bullet \frac{C_{\mathrm{GI}}}{K_{\mathrm{GI}}} Q_{\mathrm{LIV}} \cdot \frac{C_{\mathrm{LN}}}{K_{\mathrm{LIV}}} - CL_{\mathrm{LIV}} \bullet \frac{\mathrm{LIV}}{V_{\mathrm{LIV}}} \quad ; \mathrm{LIV}(0) = 0 \tag{3}$$

where CL_{LIV} is the total intrinsic clearance from the liver.

Lungs (LU):

$$\frac{d}{dt}\mathrm{LU} = Q_{\mathrm{LU}} \bullet \left(\frac{\mathrm{VEN}}{V_{\mathrm{VEN}}} - \frac{C_{\mathrm{LU}}}{K_{\mathrm{LU}}}\right); \quad \mathrm{LU}(0) = 0 \tag{4}$$

All tissues except lungs received the input from the arterial blood supply.

Other non-eliminating tissues:

$$\frac{d}{dt}\mathrm{TISSUE} = Q_{\mathrm{tissue}} \bullet \left(\frac{\mathrm{ART}}{V_{\mathrm{ART}}} - \frac{C_{\mathrm{tissue}}}{K_{\mathrm{tissue}}}\right); \quad \mathrm{TISSUE}(0) = 0 \tag{5}$$

The oral absorption model included a lumen compartment through which a fraction of dose is absorbed into the gastrointestinal compartment (FFA) by a single or multiple absorption rate constants, which were tested. For example, Eq. 6 describes the model with two different first-order absorption rate constants, $k_{A,}$ and k_{A1}, with each process associated with the fraction of the absorbed dose FAGG and (1-FAGG), respectively.

Gut:

$$\frac{d}{dt}\mathrm{GI} = \mathrm{FAA} \bullet \mathrm{ABS} + Q_{GI} \bullet \left(\frac{\mathrm{ART}}{V_{\mathrm{ART}}} - \frac{C_{\mathrm{GI}}}{K_{\mathrm{GI}}}\right) - \mathrm{CL}_{\mathrm{GI}} \bullet \frac{\mathrm{GI}}{V_{\mathrm{GI}}} \quad ; \quad \mathrm{GI}(0) = 0 \tag{6}$$

where

$$\mathrm{ABS} = D_{\mathrm{PO}} \bullet \mathrm{FAGG} \bullet e^{-k_A \bullet t} + D_{\mathrm{PO}} \bullet (1 - \mathrm{FAGG}) \bullet e^{-k_{A1} \bullet t} \tag{6a}$$

$$D_{\mathrm{PO}} = \mathrm{ORAL\ DOSE} \tag{6b}$$

During our initial analysis, we noticed by comparing the intestine data with respect to their i.v. and oral dose (Figs. 2 and 3) that SHetA2 concentrations in intestines after oral dose were greater than what could be explained based on the mass balance. We postulated that orally administered SHetA2 remains in the intestinal lumen adsorbed even with rinsing of the tissue with PBS, which could be possibly counted as the tissue concentration, as supposed to the actual amount entered into the enterocytes. To address this, we estimated the

adsorption factor (F_{ADS}) associated with the oral intestinal data and fixed at an optimal value.

The drug concentrations in each tissue were converted from ng/ml to ng/g by assuming a tissue density of 1 g/ml. Tissue concentrations were corrected for residual trapped blood using the following corrected tissue concentration (C_{tissue}) (17,21).

$$C_{tissue} = \frac{C_{tissue(measured)} \bullet V_{measured} - C_{PL} \bullet V_{measured} \bullet \frac{V_{vasc}}{V_{tissue}}}{V_{measured} - \left[V_{measared} \bullet \frac{V_{vasc}}{V_{tissue}}\right]} \quad (7)$$

where Ctissue and Ctissue(measured) are the corrected and measured tissue concentrations, $V_{measured}$ is the measured volume of collected tissue, and V_{vasc}/V_{tissue} is the fractional vascular volume of blood trapped in tissues as obtained from the literature (17,22). C_{PL} is the measured plasma concentration, which was expressed as the combined drug amount in arterial and venous pool (ART + VEN) divided by the total blood volume ($V_{ART} + V_{VEN}$).

The extent of SHetA2 tissue distribution was calculated using the biodistribution coefficient (K_{p_tissue}) in different tissues by comparing the area under the tissue or plasma concentration *versus* time curve from time 0 to infinity ($AUC_{0 \rightarrow \infty}$) using the standard non-compartmental analysis with Phoenix WinNonlin Version 6.4, (Certara USA, Inc., Princeton, NJ).

$$K_{p\ tissue} = \frac{AUC_{0 \rightarrow \infty Tissue}}{AUC_{0 \rightarrow \infty Plasma}} \quad (8)$$

The extent of SHetA2 partitioned to carcass ($K_{p\ \_\ CAR}$) was calculated based on the following equation, with the total volume of distribution (V_{ss}) that was noncompartmentally estimated:

$$V_{ss} = \sum V_{tissue} \bullet K_{p\_tissue} + K_{p\_CAR} \bullet V_{CAR} \quad (9)$$

The tissue partition coefficient values for all tissues (K_{tissue}) were also estimated and compared with calculated values ($K_{p\ \_\ tissue}$). The equations for plasma and all tissues were solved simultaneously for both oral and intravenous data to estimate the model parameters using the Maximum Likelihood estimation implemented in ADAPT 5 (Biomedical Simulations Resource, CA) (23). In this study, we have tested different model structures to depict the kinetics of tissue distribution (e.g., permeability-limited *vs.* perfusion-limited distribution model) and oral absorption (e.g., first-order absorption *vs.* zero-order absorption, single *vs.* multiple absorption phases). The best model structure was determined with the minimum value of Akaike Information Criterion (AIC). The final model was selected based on the comparison of AIC among structure models, the goodness-of-fit, weighted residual plots, and reliability of parameter estimations.

In silico Prediction of SHetA2's ADME Using Gastroplus™

We used a complementary in silico approach using Gastroplus™ 9.6 (SimulationsPlus Inc., Lancaster, CA) to investigate the significance and contributions of different pathways to elimination of SHetA2 in different species. The input data included the basic physicochemical properties of the drug, such as solubility (19.9 μg/ml), p*Ka* (= 11.1) (24), and log*P* (= 4.23, pH = 7) (24). If no experimental data were available, necessary input parameters (e.g., fraction unbound) were obtained from in silico structure-based predictions using the ADMET Predictor™ (version 8.0.4.6) module in Gastroplus. The in silico analysis also predicted intrinsic metabolic clearance due to each specific CYP enzyme in liver and intestine, and their contribution to total systemic clearance. The *in vivo* PK parameters (e.g., total systemic clearance and volumes of distribution) obtained from i.v. dosing in preclinical species (13) were entered. The default values for the physiological parameters were selected.

Sensitivity Analysis

A sensitivity analysis was conducted for each parameter. In each scenario, an individual model parameter was adjusted while all other parameters were held constant. Observations of the predicted changes in model output were recorded. The result is expressed as sensitivity coefficients which are the changes in the model output divided by changes in the parameters (25). In this study, model output is the AUC of the corresponding compartment.

RESULTS

Quantification of SHetA2 in Mouse Tissues

To quantify SHetA2 in different tissues, calibration curves were prepared in all tissues and shown to be linear within the concentration range (Figure S1). A single-point validation of the developed method was performed by spiking 1 μg/ml of SHetA2 in different tissue homogenates. These tissue homogenates were then analyzed for SHetA2 by our method to confirm the accuracy. As shown in Figure S2, the drug concentration in different tissue homogenates were accurately (80–120%) and precisely (< 15%) determined, confirming the suitability of our analytical method for SHetA2 quantification in various tissues.

Plasma and Tissue Distribution of SHetA2 in Tumor-Bearing Mice

Following i.v. administration (Fig. 3), the SHetA2 plasma concentration-time profile exhibited a multi-exponential decline with an elimination half-life of 4.5 h in tumor-bearing mice. The preliminary PK analysis of the intravenous and oral plasma data only estimated total systemic clearance (CL) of 99.7 ml/h, steady-state volume of distribution (V_{SS}) of 333.3 ml, and oral bioavailability (%F) of 22.6%. Following oral administration at a dose of 60 mg/kg, SHetA2 was rapidly absorbed into the intestines (T_{max} = 0.25 h), followed by liver, brain, kidney, and tumor (T_{max} = 0.5 h); uterus, heart, adipose tissues, and lung (T_{max} = 1 h); and spleen, muscle, skin, carcass, and fallopian tubes/ovaries (T_{max} = 2–2.5 h). As seen in the plasma, a similar half-life of 3.4–6.7 h was observed in the muscle, intestines, liver, brain, uterus, fallopian tubes/ovaries, skin, heart, and kidney indicating instantaneous distribution equilibrium in those tissues. In the spleen, tumor, adipose tissues, and lungs, there appears to be similar distribution behavior but this trend could not be confirmed due to

the lack of observed data at 24 h. SHetA2, being lipophilic in nature, was more partitioned into all the tissues (Table II) than in plasma (Figs. 2 and 3). The concentration of SHetA2 in tumors following the oral dose of 60 mg/kg was higher than the concentration in plasma and above ~ 0.37–4.6 μM, IC_{50} values for growth inhibition in the National Cancer Institute 60 cell line screen (3).

PBPK Modeling

The whole-body PBPK model (Fig. 1) was constructed to quantitatively understand the oral absorption and disposition of SHetA2 in orthotopic tumor-bearing mice after oral and i.v. administration. The perfusion-limited distribution model of which drug partitioning into the tissues is limited by the blood flow through the tissue was selected based on the physicochemical properties of SHetA2 and appropriately described SHetA2 disposition. To characterize the oral absorption, we first performed deconvolution analysis using the area function method (26) that utilizes oral and i.v plasma concentration to assess the kinetics with which SHetA2 is being absorbed (e.g., zero- *vs.* first-order, single *vs.* multiple absorption constants). The analysis revealed that the absorption rate decreases multi-exponentially (Figure S3), indicating more than one first-order rate constant involved in oral absorption. Based on the fitting of our observed data with different absorption constants, we found that SHetA2 absorption kinetics was best characterized by two first-order absorption rate constants, a slow k_A and a fast k_{A1} process with corresponding FAGG and (1-FAGG) fractions, respectively (Eq. 6), which were estimated. The selection of the final structural model was based upon evaluation of standard goodness-of-fits and AIC.

Figures 2 and 3 show the oral and i.v. data depicted by the final PBPK model. In general, there was in good agreement in individual predictions, except for i.v. skin, and tumor tissues, for which the data were scarce. The plots of standardized residuals *versus* predicted concentrations for all tissues show an unbiased distribution, indicating optimum fittings. Our analysis showed that 87% of the absorbed dose was associated with fast absorption rate constant, $k_{A1} = 1.73\ h^{-1}$, and the remaining 13% was associated with a slower absorption rate constant, $k_A = 0.18\ h^{-1}$ (Table III). We estimated the fraction of oral dose absorbed in intestines (FFA) and found that of the oral drug administered, only 22% entered the enterocytes. We have previously reported the solubility-limited absorption of SHetA2 in preclinical animal studies (13). The remainder of the administered dose may have been excreted into the feces. As previously reported from studies in dogs (10), we also observed the presence of yellow stools in feces of mice orally administered SHetA2, which is a yellow crystalline solid. Additionally, our quantitative analysis revealed that the measured intestine concentrations after an oral dose were much higher (23 folds) than the concentrations in enterocytes that might have actually contributed to the systemic absorption. This finding could possibly be attributed to drug's luminal adhesion. Thus, the oral intestine data should be interpreted with caution, especially when quantifying FFA.

The PBPK model estimated the total intrinsic clearance from the intestine and liver, and found minimal metabolism (~ 0.99 fraction survived from both sites) of SHetA2 in these metabolism sites (Table III), indicating that the major contributor to low bioavailability is the entry of SHetA2 into the enterocytes. A major contribution to model-estimated total body

clearance was found to be decomposition in venous and arterial blood (79.6 ml/h), which is in concordance with in silico assessment (Figure S4A) and reported literature (12).

Unlike a single subcutaneously implanted solid tumor, the peritoneal ovarian tumors in an orthotopic xenograft mouse model are discretely spread. Thus, we estimated tumor volume (V_{TUM}) and average blood flow to tumors (Q_{TUM}) in our model. The estimated V_{TUM} of 0.26 ml (Table III) was close to the observed total tumor weight (0.248 g) after collecting all visible tumor nodules. Similarly, the blood flow through the adipose tissues (Q_{AD}) was estimated to improve overall fitting for the observed data. We observed that the estimated Q_{TUM} (35.1 ml/h) and Q_{AD} (30.5 ml/h) were very close each other (Table III), suggesting similar perfusion through these tissues, which has relevance considering their physiological location in the peritoneum. Q_{TUM} may vary depending on the stage of tumor development. The previously reported Q_{TUM} ranges from 6 to 44 ml/h (27–30), which represents 1.2–11.7% of total blood flow. FQ_{TUM} from our study was calculated to be 9.3% which was within the range.

The PBPK model adequately described the SHetA2 concentrations in all tissues in tumor-bearing mice, and closely estimated the partition coefficients of all tissues with reasonable variability (Table II). The partition coefficient of SHetA2 in the spleen, brain, heart, and muscle were low (1.82–2.72), followed by the intestine, tumor, lung, adipose tissues, uterus, fallopian tubes/ovaries, kidney, liver, and skin having high partitioning (5.18–11.17). The calculated and model-estimated partition coefficient for the remaining body was found to be > 50, indicating a significant drug distribution into carcass. The sensitive analysis (Figure S6) also agreed $K_{carcass}$ being the most sensitive parameter. Our developed PBPK model will be useful in predicting adequate target concentrations within the organ of interest under different dosing regimens.

DISCUSSION

SHetA2 is the lead compound of Flex-Hets, a novel class of anticancer and preventive drugs inducing apoptosis that are being advanced for clinical development (31). SHetA2 has demonstrated its antitumor activity in various malignancies. A clear understanding of the drug's tissue distribution characteristics is important for establishing dose and time-response relationships in different tissues. This is the first study to determine tissue/tumor distribution of SHetA2 in tumor-bearing mice. In this work, we developed a full PBPK model that has provided insight into the absorption, distribution, and elimination of SHetA2 after oral administration.

The permeability and solubility of compounds greatly influence bioavailability and absorption rate (32). SHetA2 is a lipophilic drug with low solubility. Its measured Caco-2 permeability in the apical to basolateral direction (0.128×10^{-6} cm/s) was low (24), but the accuracy of this result was under scrutiny due to extremely low recovery in the assay. Drugs with poor aqueous solubility have limited luminal concentrations to saturate efflux transporters and thus can be subject to efflux transporter effects (32) influencing oral absorption. A bidirectional transport study that evaluated a rate of transport in the basolateral-to-apical over the apical-to-basolateral direction (i.e., efflux ratio) showed

SHetA2 with an efflux ratio of 1.56 in Caco-2 cells (24), suggesting a limited contribution of efflux transport to the intestinal permeability of SHetA2. We and others have reported that SHetA2 exhibits complex oral absorption, sensitive to solubility (10,13). The current study showed that 87% of the absorbed dose was associated with a fast first-order absorption process, which produced a rapid rise of SHetA2 concentrations in intestines within 15 min and a peak at 2 h in plasma (e.g., 5 times of the absorption half-life $\left[t_{k_{A1}}\right]$ of 0.40 h, based on $t_{k_{A1}} = 0.693/1.73$). Such absorption may be a result of the lipophilic nature of SHetA2. The 13% of the bioavailable dose was continuously absorbed through a slow first-order absorption process ($t_{k_A} = 3.85$ h) over a prolonged period. Such phenomenon might occur due to slow release of SHetA2 over time owing to limited gastrointestinal solubility (13). The oral absorption kinetics in dogs following oral dosing of SHetA2 formulated the same as in the present study were also characterized by two first-order processes (13). The estimated first-order rate constant accounting for the fast absorption in dogs was 1.12 h^{-1}, similar to k_{A1} (1.73 h^{-1}) in the present study.

From these two absorption processes, 22% of orally administered SHetA2 entered the enterocytes and the remaining 78% was likely to be adsorbed or excreted through feces, as observed in dogs (10). To account for the adsorption factor, F_{ADS} was estimated, which well fitted the oral intestinal data. Incorporation of such a parameter was based on the fact that diffusion of certain lipophilic drugs through the lumen is hindered by the hydrophilicity and viscosity of the mucus layer present on the intestinal lumen, and thus poses challenges for oral delivery of lipophilic drugs related to the harsh environment in the lumen (33). However, such a muco-adhesion barrier can improve the residence time of the local concentrations developed and increase the fraction absorbed from the mucosal surface over time, leading to prolonged absorption.

Based on our in silico analysis using ADMET Predictor, SHetA2 is likely a substrate for majority of CYP enzymes like CYP3A4, 2C19, 2C9, 2D6, and 1A2 for its metabolism (Figure S4 and S5). Since SHetA2 is highly plasma protein bound (~ 99.6%), however, the contribution of CYP enzymes to its metabolism is likely very small. The in silico assessment with SHetA2 predicted the unbound intrinsic clearance to be 340 ml/h in mice which, together with the fraction unbound and liver blood flow in mice, estimates the hepatic clearance of 1.3 ml/h (Figure S4B). This value is close to the hepatic clearance (0.79 ml/h; Table III) that was estimated based on intrinsic clearance CL_{LIV} from our PBPK model. Our PBPK and in silico analysis are in good agreement that SHetA2 is a low-extraction drug (the extraction ratio ~ 0.02). A similar phenomenon is likely responsible for low intestinal metabolism of SHetA2 (Figure S5) and thereby low extraction in the GI track. As the total bioavailability is F = FFA • F_G • F_H, where FFA is the fraction that entered into the enterocytes, F_G is the fraction that survived intestinal metabolism, and F_H is the fraction that survived hepatic metabolism, the total bioavailability (22%) will be a major contribution of FFA. The model closely predicted the observed bioavailability (22.6%).

In line with the drug's size and lipophilicity, a perfusion-limited model best described SHetA2 tissue distribution. We observed extensive distribution of SHetA2 in tumor-bearing mice in various tissues with the median tissue-to-plasma partition coefficient of 5.4. Since

gynecological cancers are the initial diseases of interest for SHetA2 development, high partitioning in tumors, uterus, and fallopian tubes/ovaries will be of great significance for pharmacodynamic measurements of relevant biomarkers in clinical trials.

The sensitive analysis indicates that in general, most tissue distribution coefficients are influential to each tissue exposure. Of those, $K_{carcass}$ was found to be the most sensitive parameter. The ADMET Predictor estimates a significant amount of SHetA2 partitioned in bone marrow. The carcass in our study was basically comprised of bones, which likely explains the high value of carcass partition coefficient estimated. The rest of the body takes around 20% of the whole-body volume which could significantly influence the drug distribution. Another sensitive parameter was drug metabolism in GI (CL_{GI}). The contribution of the gut first-pass metabolism to overall oral bioavailability of SHetA2 is, however, expected to be minimal because of high protein binding of SHetA2.

Although this model fulfills many advantages, it also has some limitations. First, while our study provided an insight into the likely contribution of different elimination pathways *in vivo*, it is still based on previous studies (12,20) that are largely qualitative. Detailed *in vitro* metabolism studies are needed to determine the involved CYP isoforms and enzyme inhibition/induction quantitatively for better prediction of potential drug-drug interactions in future clinical studies. Second, the physiological values are from non-tumor-bearing nude mice. The altered microenvironment in tumor-bearing mice (e.g., vasculature, pH, intra-tumor pressure) may alter the tissue volumes, especially for intraperitoneal organs and thus drug disposition. This could be especially important, when ascites develops in ovarian cancer-bearing nude mice, although we did not observe ascites in the present study. We performed our PK study 3 weeks after SKOV3 cell injection at which the tumors are vascularized (34). We monitored tumor development with bioluminescence imaging and our pilot study confirmed sufficient tumor mass development by 3 weeks. At the late stage of ovarian cancer as depicted in our current orthotopic xenograft model, tumors are widely spread over the peritoneal organs and abdominal walls. While our current study characterized them as a single tumor, in the future, it would be interesting to be able to discern drug distribution in tumors at different metastasized organs considering their blood flow and properties. Third, while we collected any visible tumor nodules and weighed them together, some small tumors unidentifiable with naked eyes may have been left out, and thus we estimated the tumor volume in this study. Also, the model could be further improved by incorporating the unbound fraction in tissues and blood/plasma, providing a better insight into liver and intestinal metabolism.

In the present study, we performed extensive mouse pharmacokinetic analysis of SHetA2 and developed a whole-body PBPK model to explain oral absorption and tissue distribution in tumor-bearing mice. Our developed PBPK model will be useful in assisting rational design of dosing regimens for preclinical models of several malignancies based on achieving target concentrations within the target tissues, and eventually for clinical applications. This approach is superior to optimizing dosing regimens based on plasma concentration, because drug penetration to various organs can vary widely depending on drug and tissue property. We are currently using this PBPK model to link the tumor concentration with the various pharmacodynamic responses, such as intrinsic apoptosis by measuring SHetA2 induction of

Bcl-2 degradation (35) or cell cycle arrest by measuring SHetA2 induction of CyclinD1 degradation (5) in tumor tissues following repeated oral doses. Furthermore, the PBPK model can be scaled up to predict exposures of SHetA2 at tumor/tissue sites in humans (e.g., cervical tissue and fallopian tube/ovary) for the planned phase 1 clinical study.

CONCLUSION

Our findings and developed PBPK model provide an insight into SHetA2 oral absorption and tissue distribution characteristics in tumor-bearing mice. This is the first study that characterized the oral absorption, tissue distribution of SHetA2 using a PBPK modeling approach. The model can be used to predict the drug exposure at tumors or other local sites of action for different dosing regimens, and scaled up to humans to correlate with efficacy, thereby facilitating clinical development of SHetA2. Also, it demonstrates the potential of using this model to predict the drug-drug interaction risk, guide the dosing regimen for patients with organ impairment.

Supplementary Material

Refer to Web version on PubMed Central for supplementary material.

ACKNOWLEDGMENTS

We are thankful to Dr. Anil Sood, MD Anderson Cancer Center, for providing the SKOV3-luc cells.

FUNDING INFORMATION

This work was made possible in part by the College of Pharmacy, Stephenson Cancer Center Gynecologic Cancer Program, and NIH R01s (1R01CA196200 and 1R01CA200126).

REFERENCES

1. Benbrook DM, Nammalwar B, Long A, Matsumoto H, Singh A, Bunce RA, et al. SHetA2 interference with mortalin binding to p66shc and p53 identified using drug-conjugated magnetic microspheres. Investig New Drugs. 2014;32(3):412–23. 10.1007/s10637-013-0041-x. [PubMed: 24254390]
2. Liu S, Brown CW, Berlin KD, Dhar A, Guruswamy S, Brown D, et al. Synthesis of flexible sulfur-containing heteroarotinoids that induce apoptosis and reactive oxygen species with discrimination between malignant and benign cells. J Med Chem. 2004;47(4):999–1007. 10.1021/jm030346v. [PubMed: 14761202]
3. Benbrook DM, Kamelle SA, Guruswamy SB, Lightfoot SA, Rutledge TL, Gould NS, et al. Flexible heteroarotinoids (Flex-Hets) exhibit improved therapeutic ratios as anti-cancer agents over retinoic acid receptor agonists. Investig New Drugs. 2005;23:417–28. [PubMed: 16133793]
4. Benbrook DM, Lightfoot S, Ranger-Moore J, Liu T, Chengedza S, Berry WL, et al. Gene expression analysis of biological systems driving an organotypic model of endometrial carcinogenesis and chemoprevention. Gene Regul Syst Biol. 2008;2:21–42.
5. Masamha CP, Benbrook DM. Cyclin D1 degradation is sufficient to induce G1 cell cycle arrest despite constitutive expression of cyclin E2 in ovarian cancer cells. Cancer Res. 2009;69(16):6565–72. 10.1158/0008-5472.can-09-0913. [PubMed: 19638577]
6. Guruswamy S, Lighfoot S, Gold MA, Hassan R, Berlin KD, Ivey RT, et al. Effects of retinoids on cancerous phenotype and apoptosis in organotypic cultures of ovarian carcinoma. J Natl Cancer Inst. 2001;93(7):516–25. 10.1093/jnci/93.7.516. [PubMed: 11287445]

7. Liu T, Masamha CP, Chengedza S, Berlin KD, Lightfoot S, He F, Benbrook DM. Development of flexible-heteroarotinoids for kidney cancer. Mol Cancer Ther. 2009;8(5):1227–38. 10.1158/1535-7163.MCT-08-1069. [PubMed: 19417155]
8. Doppalapudi RS, Riccio ES, Davis Z, Menda S, Wang A, Du N, et al. Genotoxicity of the cancer chemopreventive drug candidates CP-31398, SHetA2, and phospho-ibuprofen. Mutat Res. 2012;746(1):78–88. 10.1016/j.mrgentox.2012.03.009. [PubMed: 22498038]
9. Mic FA, Molotkov A, Benbrook DM, Duester G. Retinoid activation of retinoic acid receptor but not retinoid X receptor is sufficient to rescue lethal defect in retinoic acid synthesis. Proc Natl Acad Sci U S A. 2003;100(12):7135–40. 10.1073/pnas.1231422100. [PubMed: 12782789]
10. Kabirov KK, Kapetanovic IM, Benbrook DM, Dinger N, Mankovskaya I, Zakharov A, et al. Oral toxicity and pharmacokinetic studies of SHetA2, a new chemopreventive agent, in rats and dogs. Drug Chem Toxicol. 2013;36(3):284–95. 10.3109/01480545.2012.710632. [PubMed: 22947079]
11. Benbrook DM, Guruswamy S, Wang Y, Sun Z, Mohammed A, Zhang Y, et al. Chemoprevention of colon and small intestinal tumorigenesis in APC(min/+) mice by SHetA2 (NSC721689) without toxicity. Cancer Prev Res (Phila). 2013;6(9):908–16. 10.1158/1940-6207.capr-13-0171. [PubMed: 23852423]
12. Zhang Y, Hua Y, Benbrook DM, Covey JM, Dai G, Liu Z, et al. High performance liquid chromatographic analysis and preclinical pharmacokinetics of the heteroarotinoid antitumor agent, SHetA2. Cancer Chemother Pharmacol. 2006;58(5):561–9. 10.1007/s00280-006-0211-z. [PubMed: 16534614]
13. Sharma A, Benbrook DM, Woo S. Pharmacokinetics and interspecies scaling of a novel, orally-bioavailable anti-cancer drug, SHetA2. PLoS One. 2018;13(4):e0194046 10.1371/journal.pone.0194046. [PubMed: 29634717]
14. Jones HM, Chen Y, Gibson C, Heimbach T, Parrott N, Peters SA, et al. Physiologically based pharmacokinetic modeling in drug discovery and development: a pharmaceutical industry perspective. Clin Pharmacol Ther. 2015;97(3):247–62. 10.1002/cpt.37. [PubMed: 25670209]
15. Ibrahim M, Hatipoglu MK, Garcia-Contreras L. SHetA2 dry powder aerosols for tuberculosis: formulation, design, and optimization using quality by design. Mol Pharm. 2018;15(1):300–13. 10.1021/acs.molpharmaceut.7b01062. [PubMed: 29219321]
16. Sharma A, Thavathiru E, Benbrook DM, Woo S. Bioanalytical method development and validation of HPLCUV assay for the quantification of SHetA2 in mouse and human plasma: application to pharmacokinetics study. J Pharmaceut Technol Drug Res. 2017;6(1):2 10.7243/2050-120X-6-2.
17. Brown RP, Delp MD, Lindstedt SL, Rhomberg LR, Beliles RP. Physiological parameter values for physiologically based pharmacokinetic models. Toxicol Ind Health. 1997;13(4):407–84. 10.1177/074823379701300401. [PubMed: 9249929]
18. Gerlowski LE, Jain RK. Physiologically based pharmacokinetic modeling: principles and applications. J Pharm Sci. 1983;72(10):1103–27. [PubMed: 6358460]
19. Davies B, Morris T. Physiological parameters in laboratory animals and humans. Pharm Res. 1993;10(7):1093–5. [PubMed: 8378254]
20. Liu Z, Zhang Y, Hua YF, Covey JM, Benbrook DM, Chan KK. Metabolism of a sulfur-containing heteroarotionoid antitumor agent, SHetA2, using liquid chromatography/tandem mass spectrometry. Rapid Commun Mass Spectrom. 2008;22(21):3371–81. 10.1002/rcm.3744. [PubMed: 18837006]
21. Pawaskar DK, Straubinger RM, Fetterly GJ, Hylander BH, Repasky EA, Ma WW, et al. Physiologically based pharmacokinetic models for everolimus and sorafenib in mice. Cancer Chemother Pharmacol. 2013;71(5):1219–29. 10.1007/s00280-013-2116-y. [PubMed: 23455451]
22. Laurence T, Baxter HZ, Mackensen DG, Jain RK. Physiologicaly based pharmacokinetic model for specific and nonspecific monoclonal antibodies and fragments in normal tisues and human tumor xenografts in nude mice. Cancer Res. 1994;54:1517–28. [PubMed: 8137258]
23. D'Argenio DZ, Schumitzky A, Wang X. ADAPT 5 User's guide: pharmacokinetic/pharmacodynamic systems analysis software. Los Angeles: Biomedical Simulations Resource; 2009.
24. Banerjee AK, Frost S, Frost K, Thomas S, Metcalfe P, Kapetanovic IM, et al. Development of more bioavailable orally absorbed chemopreventive agents from leads derived from natural sources

Potential challenges. Presented at the 49th Annual Meeting of the Society of Toxicology, March 7–11, 2010, Salt Lake City, Utah, USA 2010.

25. Plowchalk DR, Andersen ME, Bogdanffy MS. Physiologically based modeling of vinyl acetate uptake, metabolism, and intracellular pH changes in the rat nasal cavity. Toxicol Appl Pharmacol. 1997;142(2):386–400. 10.1006/taap.1996.8052. [PubMed: 9070362]
26. Cheng H, Staubus AE, Shum L. An area function method for estimating the apparent absorption rate constant. Pharm Res. 1988;5(1):57–60. [PubMed: 3244611]
27. Davda JP, Jain M, Batra SK, Gwilt PR, Robinson DH. A physiologically based pharmacokinetic (PBPK) model to characterize and predict the disposition of monoclonal antibody CC49 and its single chain Fv constructs. Int Immunopharmacol. 2008;8(3):401–13. 10.1016/j.intimp.2007.10.023. [PubMed: 18279794]
28. Baxter LT, Zhu H, Mackensen DG, Jain RK. Physiologically based pharmacokinetic model for specific and nonspecific monoclonal antibodies and fragments in normal tissues and human tumor xenografts in nude mice. Cancer Res. 1994;54(6):1517–28. [PubMed: 8137258]
29. Kim SG, Ackerman JJ. Quantitative determination of tumor blood flow and perfusion via deuterium nuclear magnetic resonance spectroscopy in mice. Cancer Res. 1988;48(12):3449–53. [PubMed: 2836055]
30. Rogers W, Edlich RF, Aust JB. Tumor blood flow. II. Distribution of blood flow in experimental tumors. Angiology. 1969;20(7):374–87. 10.1177/000331976902000702. [PubMed: 5797931]
31. Liu S, Zhou G, Lo SNH, Louie M, Rajagopalan V. SHetA2, a new cancer-preventive drug candidate. Anti-cancer Drugs: Nature, Synthesis and Cell 2016;67.
32. Shugarts S, Benet LZ. The role of transporters in the pharmacokinetics of orally administered drugs. Pharm Res. 2009;26(9):2039–54. 10.1007/s11095-009-9924-0. [PubMed: 19568696]
33. Sigurdsson HH, Kirch J, Lehr CM. Mucus as a barrier to lipophilic drugs. Int J Pharm. 2013;453(1):56–64. 10.1016/j.ijpharm.2013.05.040. [PubMed: 23727593]
34. Steinkamp M, Kanigel-Winner K, Davies S, Muller C, Zhang Y, Shirinifard A, et al. Ovarian tumor attachment, invasion, and vascularization reflect unique microenvironments in the peritoneum: insights from xenograft and mathematical models. Front Oncol. 2013;3:97 10.3389/fonc.2013.00097. [PubMed: 23730620]
35. Liu T, Hannafon B, Gill L, Kelly W, Benbrook D. Flex-Hets differentially induce apoptosis in cancer over normal cells by directly targeting mitochondria. Mol Cancer Ther. 2007;6(6):1814–22. 10.1158/1535-7163.MCT-06-0279. [PubMed: 17575110]

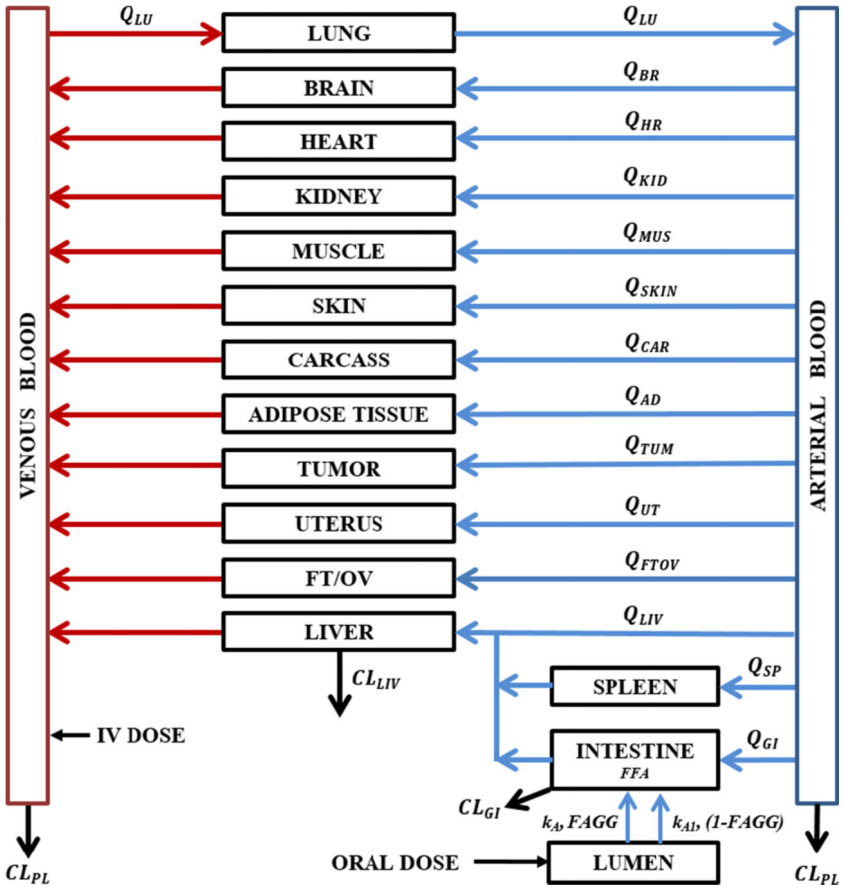

Fig. 1.

A whole-body PBPK model for SHetA2 in tumor-bearing mice. The model comprises 14 perfusion-limited tissue compartments parameterized by tissue volumes (V_{tissue}), blood flow rates (Q_{tissue}), and the drug-dependent tissue/blood partition coefficient (K_{tissue}). The elimination of SHetA2 occurs through plasma by decomposition (CL_{PL}) and metabolism in liver (CL_{LIV}) and gut (CL_{GI}). The oral dose enters into a lumen compartment through which a fraction of dose is absorbed into the gut compartment (FFA) by two different first-order absorption rate constants, k_A and k_{A1}, with each process associated with the fraction of the absorbed dose FAGG and (1-FAGG), respectively. The values of blood flow (Q_{tissue}) and volumes of organs/tissues (V_{tissue}) were obtained from the literature and listed in Table I

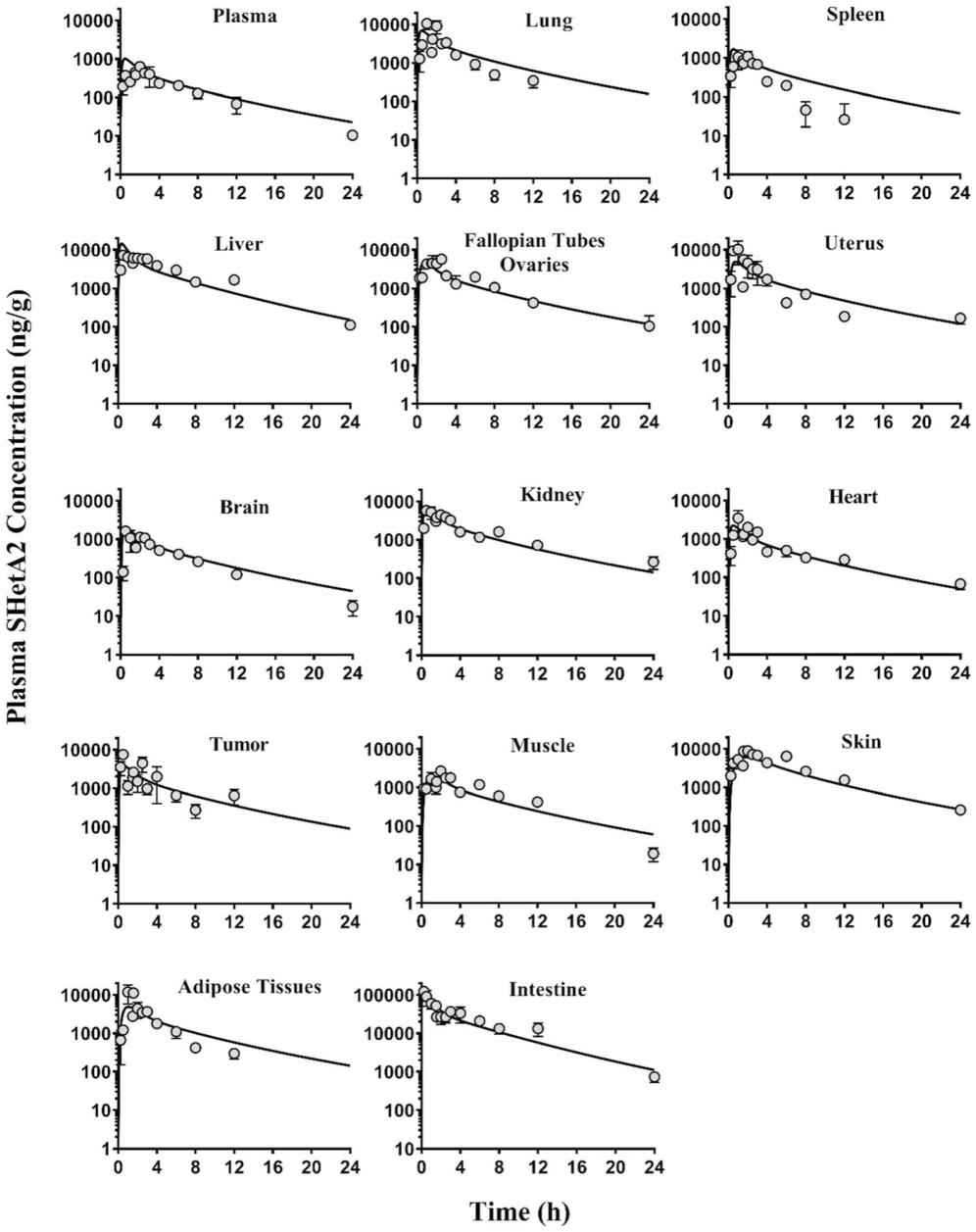

Fig. 2.

The concentration-time profiles of SHetA2 in tissues and plasma after oral administration of 60 mg/kg SHetA2 in SKOV3 tumor-bearing mice. The symbols are the observed data from three mice at each time point. The data are presented as mean ± SEM. The lines represent the model-predicted concentrations. Note that the *y*-axis scale for intestine is different from that of the other panels

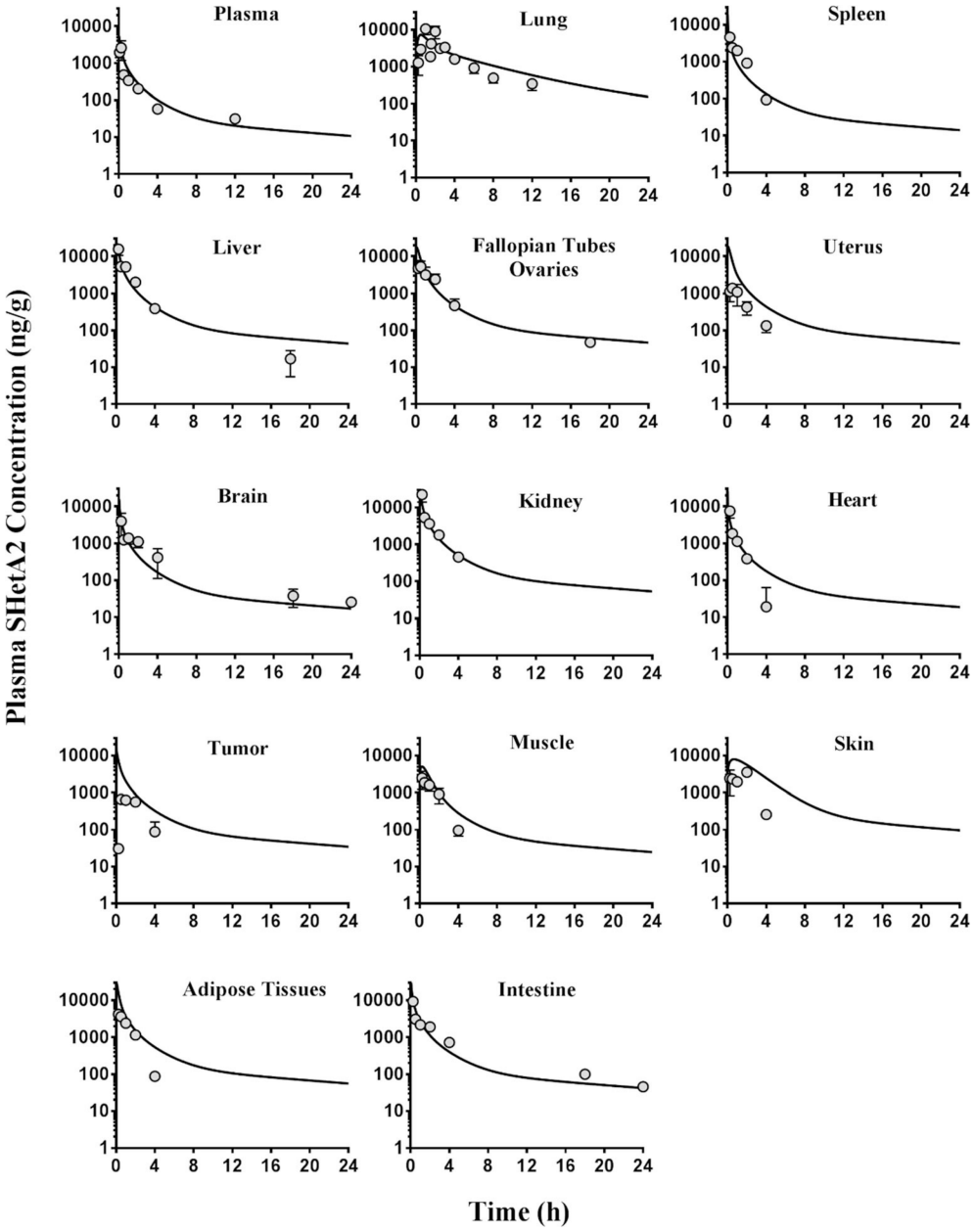

Fig. 3.

The concentration-time profiles of SHetA2 in tissues and plasma after intravenous administration of 10 mg/kg SHetA2 in SKOV3 tumor-bearing mice. The symbols are the observed data from three mice at each time point. The data are presented as mean ± SEM. The lines represent the model-predicted concentrations

Table I.

List of Physiological Parameters for Blood Flow and Organ Weight for a Nude Mouse

Organ	**Symbol**	**% of cardiac output (FQ_{tissue}) Cardiac output (CO) = 375 ml/h**	**% of body weight (FV_{tissue}) Body weight (BW) = 22.3 g**
Lung	LU	100	0.73
Artery	ART	100	2.24
Venous pool	VEN	100	4.56
Adipose	AD	$\%FQ_{AD} = Q_{AD}{}^{a}/CO$	6.98
Muscle	MUS	13.34	38.4
Liver	LIV	25	5.49
Intestine	GI	21.98	4.22
Spleen	SP	1.34	0.35
Heart	HR	4.13	0.50
Brain	BR	6.72	1.65
Kidney	KID	18.81	1.67
Skin	SK	8.93	16.5
Fallopian/ovaries	FTOV	0.48	0.27
Uterus	UT	0.48	0.26
Tumor	TUM	$\%FQ_{TUM} = Q_{TUM}{}^{b}/CO$	$\%FV_{TUM} = V_{TUM}{}^{c}/BW$
Carcass	CAR	$22.11 - FQ_{TUM} - FQ_{AD}$	$16.18 - FV_{TUM}$

Estimated parameters for blood flow for ^{a} adipose tissue and ^{b} *tumor, and* ^{c} *volume of tumor*

Table II.

Summary of Experimental and Estimated Partition Coefficients from the PBPK Model

Organs/tissues	Observed biodistribution coefficient, K_{p_tissue}	Model-estimated partition coefficient, K_{tissue} (%CV)
Spleen	1.38	1.68 (14.2)
Brain	2.03	2.00 (13.7)
Heart	4.60	2.33 (14.2)
Muscle	4.61	2.63 (13.5)
Intestine	4.77	4.95 (75.5)
Tumor	5.58	4.14 (14.5)
Lung	7.69	6.28 (15.0)
Adipose tissue	7.78	6.35 (14.5)
Uterus	7.85	5.44 (13.7)
Fallopian tubes/ovaries	8.64	5.26 (13.5)
Kidney	10.8	6.45 (14.1)
Liver	16.2	5.62 (30.3)
Skin	21.2	10.9 (14.4)
Carcass	50.9	80.3 (69.3)

Table III.

The Estimated Parameters from the Whole-Body PBPK Model Using Intravenous and Oral Data of SHetA2 Plasma Concentration-Time Profiles in Tumor-Bearing Mice

Parameters	Parameter description	Value (%CV)
CL_{LIV} (ml/h)	Hepatic intrinsic clearance	0.80 (> 100)
CL_{GI} (ml/h)	Gut intrinsic clearance	0.34 (> 100)
CL_{PL} (ml/h)	Plasma clearance	39.8 (51.1)
k_A (h^{-1})	Slow first-order absorption rate constant	0.18 (13.0)
k_{A1} (h^{-1})	Fast first-order absorption rate constant	1.73 (27.0)
FAGG	Fraction of dose followed slow absorption from lumen	0.13 (5.30)
FFA	Fraction of dose absorbed into intestine	0.22 (12.1)
V_{TUM} (ml)	Tumor volume	0.26 (> 100)
Q_{TUM} (ml/h)	Blood flow through tumor nodules	35.1 (34.6)
Q_{AD} (ml/h)	Blood flow through adipose tissues	30.5 (37.2)